Characterization of the melt removal rate in laser cutting of thick-section stainless steel

Catherine Wandera
Department of Mechanical Engineering, Lappeenranta University of Technology, Tuotantokatu 2, Lappeenranta FIN-53850, Finland

Veli Kujanpaa
Department of Mechanical Engineering, Lappeenranta University of Technology, Tuotantokatu 2, Lappeenranta FIN-53850, Finland and VTT Technical Research Centre of Finland, Tuotantokatu 2, Lappeenranta FIN-53850, Finland

(Received 2 December 2009; accepted for publication 4 April 2010; published 23 July 2010)

The efficiency of the laser cutting process depends on both the rate of melting and rate of melt removal from the cut kerf. The depth of flow separation and the dross attachment on the lower cut edge relate to the efficiency of the melt removal process and can be used to characterize the rate of melt removal from the cut kerf. The melt flow velocity and melt film thickness are formulated in this study by consideration of the fundamentals of viscous incompressible fluid flow. The calculated melt flow velocity and melt film thickness are correlated with the depth of flow separation on the 10 mm stainless steel AISI 304 (EN 1.4301) laser cut edge. The effects of process parameters—including assist gas pressure, nozzle diameter, nozzle standoff, focal point position, and cutting speed—on the depth of flow separation and the dross attachment on the lower cut edge are investigated. The assist gas pressure, nozzle diameter, and focal point position are found to significantly affect the efficiency of melt removal from the cut kerf. © *2010 Laser Institute of America.*

Key words: laser cutting, melt removal rate, thick-section stainless steel, melt velocity, boundary layer thickness, flow separation

I. INTRODUCTION

Laser cutting of sheet and plate metal is one of the major applications of high power lasers with steels—both low alloyed steels and stainless steels—taking a majority share of metals that are usually laser cut in industry. The high power laser systems with high beam quality provide the necessary power intensity required for cutting of thick-section stainless steel using inert assist gas and high cutting speeds can be realized. In principle laser cutting of stainless steel using an inert assist gas jet (usually nitrogen) is accomplished by two mechanisms, namely, melt formation through absorption of the incident laser beam and melt removal from the cut kerf through the action of the high pressure assist gas jet. After initiation of the laser cutting process, continuous melt formation occurs through absorption of the incident laser beam at the melt surface in the cutting front as the molten material is continuously sheared and accelerated down the cut kerf by the pressurized assist gas jet until the melt is ejected from the cut kerf. Olsen[1,2] described the fundamental mechanisms of the cutting front formation in laser cutting and estimated the melt film thickness at the cutting front by considering the molten film formed by thermal conduction and the acceleration of the molten material by the cutting gas pressure. He reported that the limitation in the melt removal rate due to the limited gas pressure in the cut kerf is the practical limiting factor of the laser cutting process rather than the power or intensity of the available laser beams.[1] The melt removal rate is especially critical during laser cutting of thick-section metal because of the high amount of melt generated in the narrow thick-section laser cut kerf.

Laser cut quality is strongly affected by the hydrodynamic interaction of the assist gas jet with the molten material in the cut kerf. The rate of melt removal depends on the boundary layer flow which is the region close to the kerf wall where the viscous effects are dominant and the velocity profile is due to the shear stress. It is desirable that a laminar boundary layer flow is sustained along the whole cut thickness so that the laminar flow runs attached to the kerf wall and effectively sweeping away the molten material. For good cutting quality, a laminar flow regime can be maintained throughout the cut depth in thin sheet cutting with a small cut kerf but thick plate cutting requires a larger kerf width to allow the flow to be laminar up to larger cut depths.[3] Poor cut quality results when the melt flow regime transitions into a turbulent boundary layer before it clears the bottom cut edge.

The gas flow dynamics inside the laser cut kerf constitute an important factor in the resulting cut quality so that much effort has been oriented toward improving the capability of the assist gas to remove the molten material from the cut kerf. Gross *et al.*[4] investigated the melt flow pattern inside narrow thick-section kerfs using numerical simulation techniques and identified wave structures in the melt flow which reduced the drag and pressure forces available for melt acceleration and subsequent expulsion. They reported that a higher assist gas pressure enhanced a more homoge-

neous acceleration with less integration of the flow down the kerf leading to less or delayed build up of melt. Sparkes *et al.*[5,6] reported that the major factor limiting the cut quality in inert gas laser cutting of (6–10)-mm-thick stainless steel plates using the high brightness fiber laser was the difficulty in obtaining full melt ejection through the narrow cut kerfs. Duan *et al.*[7] reported that the gas flow field inside the laser cut kerf strongly depends on the geometric shape of the cutting front that is determined by the input laser cutting parameters such as laser power, cutting speed, and focus position. Increase in the inlet pressure, nozzle exit diameter, and overlap of the nozzle with the cut kerf improved the gas flow field inside the kerf and enhanced efficient melt removal. Tani *et al.*[8] reported that dross formation was dependent on the surface tension and occlusion of the kerf bottom through an excess of liquid. Man *et al.*[9] used shadowgraphic techniques to study the gas jet patterns inside the cut kerf for supersonic and subsonic (conical) nozzle tips under high inlet stagnation pressure. They reported that the conical nozzle tip produced a radically expanding flow and the behavior of the gas jet inside the kerf worsened with increase in stand-off distance while a properly designed supersonic nozzle tip produced a gas flow with uniform distribution so that the behavior of the gas jet inside the kerf was independent of the variations in stand-off distance. The gas jet behavior inside the cut kerf was influenced by the kerf width and workpiece thickness. Man *et al.*[10] demonstrated that a proper design of the supersonic nozzle for high gas pressure laser cutting based on the theory of gas dynamics ensures that the exit jet with high momentum and good uniform boundary can be obtained so that the tolerance of the stand-off distance between the nozzle tip and the workpiece can be increased.

High gas pressures are utilized during laser cutting of thick-section metal with an inert assist gas jet. However, a supersonic gas jet delivered through the commonly used conical gas nozzles results in a series of shock structures in the gas flow due to the adjustment of the higher pressure at the nozzle exit to the atmospheric ambient pressure. Chen *et al.*[11] reported that the interaction of the shock waves in a supersonic gas jet contributes to a large reduction in the stagnation pressure at the cutting front thus reducing the material removal capability of the assist gas jet. The shock structure is influenced by the gas pressure and nozzle stand-off distance. Fieret *et al.*[12] reported that the complex shocks structure in a supersonic gas jet results in various high pressure regions in the gas flow but with limited tolerance in each high pressure region. Jun *et al.*[13] used numerical simulations to study the effect of stand-off distance on the mass flow rate and the axial thrust in the cut kerf and reported that stand-off distance has great effect on the shock structure and the jump and fluctuation of the thrust for different exit Mach number. The dynamic characteristics of gas jets from supersonic nozzles for high pressure gas laser cutting and the design of optimized supersonic nozzles capable of delivering a supersonic exit jet with high momentum and uniform boundary have been addressed by various authors.[14–16] Quintero *et al.*[17] demonstrated the benefits of an off-axis nozzle for molten material removal over the conventional coaxial assist gas jet. However, the selection of the inclination angle between the laser beam axis and the gas jet as well as the position of the impinging point of the gas jet with regards to the incidence point of the laser beam are crucial to the cut quality. Riveiro *et al.*[18] demonstrated the use of a supersonic cutting head with an off-axis gas jet for the cutting of aluminum alloy and reported that more superior cut quality was achieved than with the conventional coaxial conical cutting head. Duan *et al.*[19] reported that the tendency for boundary layer separation which reduces the cut edge quality is influenced by the curved shock formed in the flow field inside the cut kerf; and the curved shock becomes stronger with larger inclination angle of the cutting front. The pressure gradient in the cut kerf is influenced by the shock-structure in the assist gas flow; the normal situation is the decreasing pressure down the kerf, however, a sudden increase in pressure results when the gas flow passes the point of incidence of the curved shock resulting in a reduction in the flow velocity and an increase in the boundary layer thickness.[19,20] In order to maintain a high cutting quality, a laminar boundary layer melt flow must be maintained throughout the cut depth. Schulz *et al.*[21] described the time dependent interaction of the contributing transport processes during laser cutting. They reported that the onset of ripple formation on the cut edge is caused by the time-dependent movement of the width of the cutting front as a response to fluctuations of the processing parameters.

This paper investigates the rate of melt removal from the cut kerf during laser cutting of thick-section stainless steel using an inert assist gas jet and identifies the process parameters that influence the rate of melt removal from the cut kerf. The melt flow velocity and the melt film thickness are modeled by applying the principles of conservation of mass and momentum to the boundary layer flow. The model result is correlated with the cut quality obtained in the experimental investigation of laser cutting of 10 mm stainless steel AISI 304 (EN 1.4301) plate with nitrogen as assist gas.

II. MODELING OF LAMINAR BOUNDARY LAYER MELT FLOW

The laser cutting front is formed by a thin melt film which propagates through the material with a velocity that depends on the energy input, thermal properties of the workpiece material, and the molten material removal mechanisms.

A. Melt flow velocity formulation

As the laser cutting process progresses, the entire melt surface is in contact with the gas jet as shown in the schematic representation of the laser cutting front in Fig. 1(a). The melt velocity profile in the boundary layer is presented in Fig. 1(b). The x-axis is directed in the cutting direction, y is the coordinate perpendicular to the cutting front, and z coordinate is along the cut depth.

To specify the melt flow problem, the following assumptions are made:

(i) The melt film thickness is much smaller than the kerf width and the workpiece thickness so that the melt

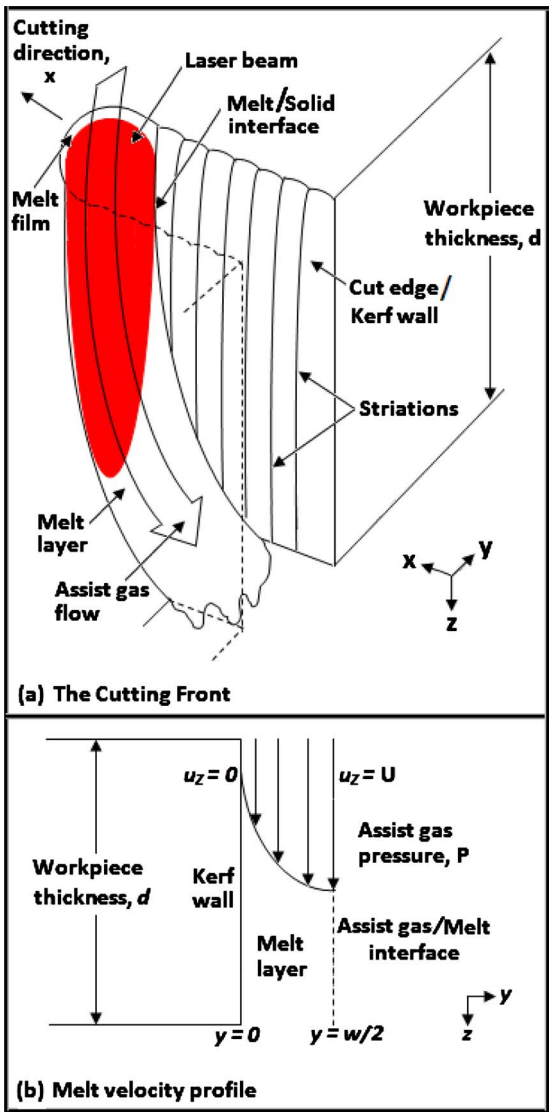

FIG. 1. The cutting front and melt velocity profile in the boundary layer (w is kerf width).

ejection from the cut kerf can be taken as a two-dimensional problem.

(ii) The cutting front inclination is negligible.

(iii) There is no substantial vaporization and the melt ejection is mainly directed down the cut kerf in the z direction.

(iv) The melt is modeled as a viscous incompressible fluid; and the melt flow is considered to be laminar and steady.

(v) The melt flow velocity at any downstream position z follows a smooth profile from zero at the melt/solid interface (i.e., kerf wall) to the maximum melt velocity U at the gas/melt interface [see Fig. 1(b)].

Assumptions (i)–(v) given above are reasonable for the case of laser cutting of thick-section metal using an inert assist gas jet whereby lower cutting speeds are applied because of the higher laser power requirement.

The two-dimensional continuity equation (conservation of mass) for a steady-state incompressible melt flow is given by Eq. (1) (Refs. 22 and 23)

$$\frac{\partial u_y}{\partial y} + \frac{\partial u_Z}{\partial z} = 0, \tag{1}$$

where u_y and u_z are components of the melt velocity vector u in y and z directions, respectively.

The melt ejection from the laser cut kerf is mainly driven by two forces exerted by the assist gas jet which include: the shear force at the gas/melt interface and the pressure gradient.[24] The shear stress, τ exerted on the melt layer by the assist gas jet is given as

$$\tau = \left. \eta \frac{\partial u_z}{\partial y} \right|_{y=0}, \tag{2}$$

where η is the gas viscosity, u_z is the melt velocity, and y is the coordinate perpendicular to the cutting front.

The two-dimensional Navier-Stokes equations (conservation of momentum) for motion of a fluid element are given by Eqs. (3a) and (3b). P is the assist gas pressure, ρ is melt density, and μ is the melt kinematic viscosity;[22,23]

$$\rho\left(u_y \frac{\partial u_y}{\partial y} + u_z \frac{\partial u_y}{\partial z}\right) = -\frac{\partial P}{\partial y},$$

$$\mu\left(\frac{\partial^2 u_y}{\partial y^2} + \frac{\partial^2 u_y}{\partial z^2}\right), \tag{3a}$$

$$\rho\left(u_y \frac{\partial u_z}{\partial y} + u_z \frac{\partial u_z}{\partial z}\right) = \frac{\partial}{\partial y}\left(\eta \frac{\partial u_z}{\partial y}\right) - \frac{\partial P}{\partial z} + \mu\left(\frac{\partial^2 u_z}{\partial y^2} + \frac{\partial^2 u_z}{\partial z^2}\right). \tag{3b}$$

When there is no substantial vaporization in the cut kerf, the melt ejection is mainly directed through the bottom of the cut kerf (z direction) and the transverse velocity component u_y will be negligible. Continuity Eq. (1) reduces to $\partial u_Z / \partial z = 0$ and the boundary-layer Eqs. (3a) and (3b) reduce to Eqs. (4a) and (4b), respectively:

$$-\frac{\partial P}{\partial y} = 0, \tag{4a}$$

$$\frac{\partial}{\partial y}\left(\eta \frac{\partial u_z}{\partial y}\right) - \frac{\partial P}{\partial z} + \mu \frac{\partial^2 u_Z}{\partial y^2} = 0. \tag{4b}$$

The pressure gradient inside the cut kerf is given as[20]

$$\frac{\partial P}{\partial z} = -\frac{1}{2}\frac{\rho_g U_g^{\,2}}{d}, \tag{5}$$

where ρ_g is the gas density, U_g is the characteristic gas velocity inside the cut kerf, and d is the workpiece thickness.

The gas velocity U_g in the cut kerf can be estimated using the Bernoulli equation as

$$P = \rho_g U_g^{\,2}/2.$$

Putting Eq. (5) into Eq. (4b) gives

$$\frac{\partial^2 u_z}{\partial y^2} = -\left(\frac{1}{\eta + \mu}\right)\left(\frac{\rho_g U_g^{\,2}}{2d}\right). \tag{6}$$

During laser cutting, the velocity of the melting front is largest at the central region of the cut kerf[1,2] and the melt flow

TABLE I. Physical properties of stainless steel and nitrogen gas (Refs. 25 and 26).

Property	Stainless steel	Nitrogen
Density (kg/m^3)	8030	1.185
Viscosity (mPas)	10.26 (at 1439 °C)	0.0165

velocity u_z must then be highest at the central region so as to maintain a steady cutting process. The maximum melt velocity is obtained at the gas/melt interface and the melt velocity is zero at the melt-solid interface due to the no-slip condition at the kerf wall. Therefore, integrating Eq. (6) and noting that $\partial u_z/\partial y=0$ at $y=w/2$ (i.e., u_z is maximum at the central region of the cut kerf where the melt is in contact with the gas jet) and $u_Z=0$ at $y=0$ (i.e., no-slip condition at the kerf wall), the expression for the melt flow velocity profile is given as

$$u_z=\left(\frac{1}{\eta+\mu}\right)\left(\frac{\rho_g U_g{}^2}{4d}\right)(wy-y^2) \tag{7}$$

and the maximum melt flow velocity U at the gas/melt interface (at $y=w/2$) is

$$U=\left(\frac{1}{\eta+\mu}\right)\left(\frac{\rho_g U_g{}^2}{16d}\right)w^2. \tag{8}$$

B. Melt film thickness

Considering a unit thickness melt film thickness, the total flow Q is given as

$$Q=\int_0^w u_z dy$$

and the mean melt velocity u_m averaged across the cut kerf is

$$u_m=\frac{Q}{w}=\left(\frac{1}{\eta+\mu}\right)\left(\frac{\rho_g U_g{}^2}{24d}\right)w^2.$$

For a steady laser cutting process, the mass balance between the rate of melting and the rate of melt removal from the cut kerf is given as

$$\rho u_m t w=\rho V d w,$$

where ρ is melt density, u_m is the mean melt velocity, t is the melt film thickness, w is the kerf width, and d is the workpiece thickness.

The melt film thickness t is

$$t=\frac{24\upsilon d^2(\eta+\mu)}{\rho_g U_g{}^2 w^2}. \tag{9}$$

The physical properties of the stainless steel workpiece and nitrogen gas given in Table I are used to model the melt flow velocity U and melt film thickness t using Eqs. (8) and (9), respectively.

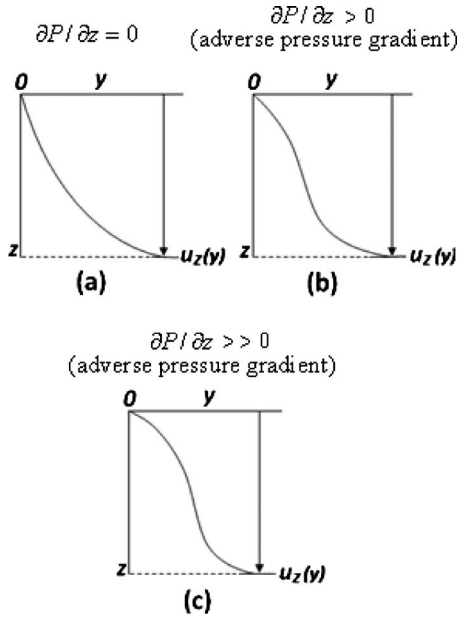

FIG. 2. Effect of pressure gradient on the flow velocity profile and separation.

C. Separation and transition of flow

From the boundary-layer Eq. (4b), we have at the kerf wall[22]

$$\frac{\partial P}{\partial z}=(\eta+\mu)\left(\frac{\partial^2 u_z}{\partial y^2}\right)_0. \tag{10}$$

It follows from Eq. (10) that in the case of a zero external pressure gradient (i.e., $\partial P/\partial z=0$), $(\partial^2 u_Z/\partial y^2)_0=0$ and the velocity gradient will take the preferable general form where $\partial u_Z/\partial y$ is greatest at the kerf wall and falls steadily to zero at the outer edge of the boundary layer as shown in Fig. 2(a). However, if there is an adverse pressure gradient in the cut kerf (i.e., $\partial P/\partial y>0$), $(\partial^2 u_Z/\partial y^2)_0$ will be positive and $\partial u_Z/\partial y$ will first increase with distance from the kerf wall before it starts to fall off to zero as shown in Fig. 2(b). Under extreme conditions of adverse pressure gradient, the velocity profile becomes increasingly distorted until the velocity gradient at the kerf wall $(\partial u_Z/\partial y)_0$ is zero [see Fig. 2(c)] and at this point separation of melt flow from the kerf wall occurs. There will be a back-flow adjacent to the kerf wall downstream from the separation point and the flow transitions into a turbulent flow in the boundary layer.

The transition to turbulent flow in the boundary layer can take place even when there is no adverse pressure gradient, for example, disturbances in a laminar boundary layer can become amplified until turbulence is developed.

III. EXPERIMENTAL PROCEDURE

A fiber laser (IPG YLR 5000) delivering a maximum output power of 5 kW at cw mode was used for performing the cutting tests on 10 mm stainless steel AISI 304 (EN 1.4301) plate with nitrogen assisting gas and cutting parameters given in Table II. The UTHSCSA ImageTool program was used to measure the kerf width from digital images of

TABLE II. Cutting parameters.

Property	Units	Value
Laser power	kW	2–5
Cutting speed	m/min	0.2–1.8
Nozzle diameter	mm	1.0–2.5
Gas pressure	bar	4–20

the cut kerfs obtained using an optical microscope-camera combination. Similarly the boundary layer separation point on the cut edges was measured from digital images of the cut edges.

IV. RESULTS AND DISCUSSION

A. Features on the cut edge

The main features on the thick-section stainless steel laser cut edge that signify the efficiency of melt removal from the cut kerf include the boundary layer separation point and the dross attachment on the lower cut edge. The profile of the cut edges shows that the melt flow starts out from the top of the cut kerf as a laminar boundary layer flow in which the melt streamlines follow straight paths. As the melt flow progresses down the cut kerf, the boundary layer thickness increases and a point is reached where the flow regime transitions into a turbulent boundary layer flow in which the melt particles move in haphazard paths as shown by the nature of the streamlines in Fig. 8. The depth of flow separation indicates the distance from the top of the cut kerf where boundary layer separation occurs as the laminar boundary layer transitions into a turbulent boundary layer (see Fig. 3). The striation pattern above the boundary layer separation point is usually uniform following straight contours along the cut thickness but the striation pattern below the separation line is irregular with slanting contours.

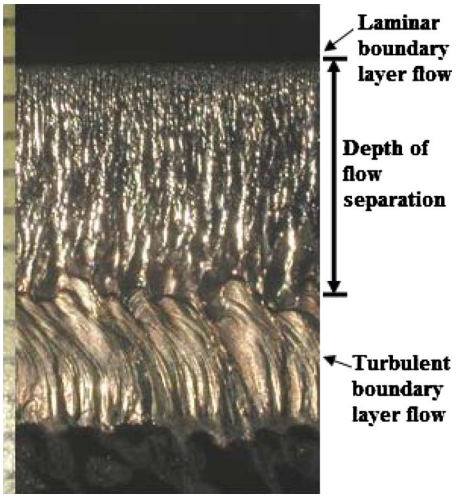

FIG. 3. Definition of depth of flow separation.

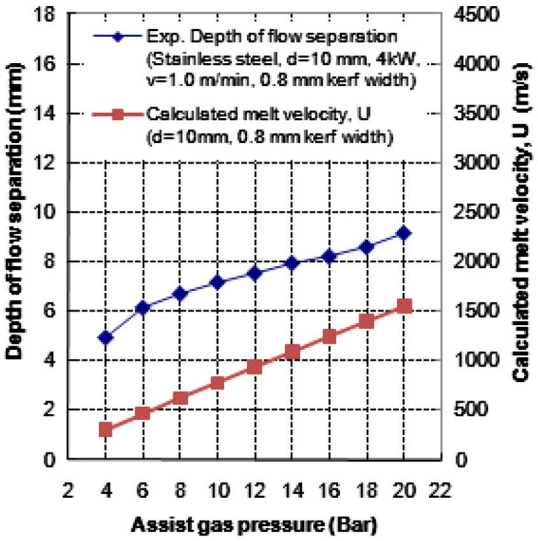

(a) Depth of flow separation and melt velocity

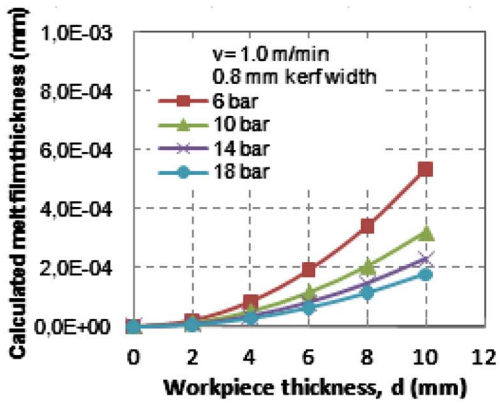

(b) Melt film thickness along cut thickness

FIG. 4. Correlation of depth of flow separation with calculated melt velocity and melt film thickness.

B. Comparison of the model and experimental results

The model and experimental results show the influence of the assist gas pressure and cut kerf width on the rate of melt removal from the cut kerf (see Figs. 4 and 5). With increase in assist gas pressure, Fig. 4 shows that melt flow velocity increases and the melt film thickness decreases so that the boundary layer separation point moves down the cut kerf. An increase in cut kerf width results in an increase in the melt flow velocity and a reduction in the melt film thickness (Fig. 5) and the boundary layer separation point moves down the cut kerf. The experimental investigation also shows that the dross attachment on the lower cut edge reduces with increase in assist gas pressure and cut kerf width.

C. Effect of assist gas pressure

The position of the boundary layer separation point moves closer to the bottom cut edge with increase in assist gas pressure (see Fig. 4) due to an increase in the Reynolds number of the melt flow. The inertial force exerted on the melt film by the assist gas is higher with increase in assist

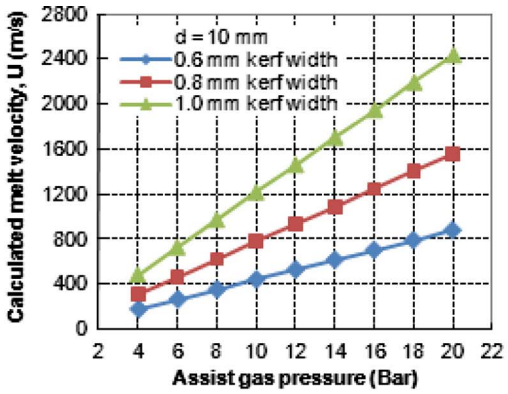

(a) Melt velocity with assist gas pressure

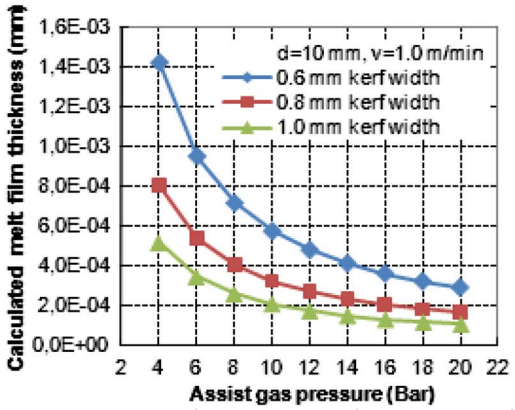

(b) Melt film thickness with assist gas pressure

FIG. 5. Calculated melt velocity and melt film thickness with assist gas pressure and cut kerf width.

gas pressure resulting in a thinner boundary layer thickness and the laminar boundary layer flow can be sustained over a longer distance down the cut edge. When the boundary layer is thin, the velocity gradient (du_Z/dy) normal to the flow is large and a large shear stress, τ_0 (where $\tau_0 = \eta du_Z/dy$) is exerted at the kerf wall by the assist gas. The corresponding shear force is large enough to exert the necessary drag on the melt close to the kerf wall and maintain a laminar flow regime as the viscous shear stresses hold the melt particles in a constant motion within layers. With low assist gas pressure, the melt flow is sluggish so that the viscous forces in the boundary layer will be more significant and the boundary layer thickness increases rapidly. As the boundary layer thickness increases, the velocity gradient becomes smaller and the viscous shear stresses decrease until they are no longer enough to drag the slow melt particles close to the kerf wall in layers and the laminar boundary layer melt flow rapidly transitions into a turbulent boundary layer. In the turbulent boundary layer, the melt particles rotate in such a way that the melt particles from the fast moving region move to the region where the particles are slower and the slower melt particles move to the faster moving region with the net effect of an increase in momentum in the boundary layer.

The viscous forces in the boundary layer flow and the pressure drop down the thick-section cut kerf reduce the melt removal rate at the lower cut section resulting in a melt flow separation and dross attachment on the lower cut edge. As the boundary layer thickness increases down the cut thickness due to deceleration of the melt film by friction between the melt layers close to the kerf wall, flow separation occurs when the melt flow regime in the boundary layer transitions from a laminar flow to turbulent boundary layer flow. Also surface tension retards the melt from clearing the lower cut edge causing dross attachment on the lower cut edge.

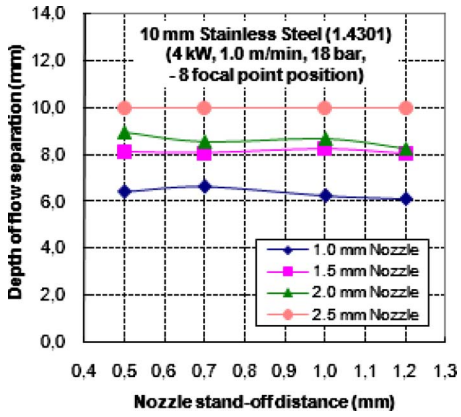

FIG. 6. Depth of flow separation with nozzle stand-off distance for different nozzle sizes.

D. Effect of nozzle diameter and nozzle standoff distance

The nozzle size has a significant effect on the depth of flow separation but the nozzle standoff distance did not significantly affect the depth of flow separation (see Fig. 6).

The nozzle diameter determines the mass flow rate of the assist gas delivered into the cut kerf and influences the inertial force exerted by the assist gas at the gas/melt interface. A larger nozzle diameter increases the mass flow rate of the assist gas in the cut kerf resulting in a higher inertial force exerted by the assist gas on the gas/melt interface and subsequently a smaller boundary layer thickness. The effect is that the melt flow will progress down the cut kerf for a longer distance without flow separation and with lower dross attachment on the lower cut edge (see Fig. 7) indicating that a larger nozzle diameter gives a higher melt removal rate and better cut edge quality.

E. Effect of focal point position

The narrow cut kerfs produced when the focal point position is located closer to the workpiece top surface results in reduced melt removal rate and flow separation occurs before the melt clears the bottom cut edge (Fig. 8). Clean cut edges—with minimal dross attachment and with the depth of flow separation close to the bottom edge of the workpiece—are obtained when the focal point position is located close to the bottom edge of the workpiece or above the workpiece top surface provided that the power intensity on the workpiece is sufficient to achieve complete penetration of

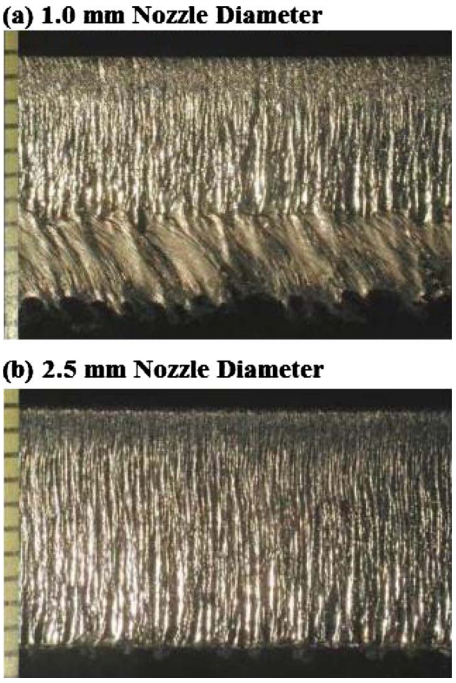

FIG. 7. Effect of nozzle size on flow separation depth (4 kW, 1.0 m/min, 18 bar, −8 focal point position).

the workpiece. The wider cut kerfs produced with the defocus focus positions enhance the melt removal rate so that the melt flow clears the bottom cut edge before flow separation occurs. Penetration of the 10 mm stainless steel workpiece at 1.0 m/min with 4 kW laser power could not be achieved with the focal point position located at 6 mm above the workpiece top surface due to the reduced power intensity at the workpiece.

The main factors to be considered when deciding the optimum focal point position in thick-section metal cutting include the required power intensity to penetrate the workpiece at a high cutting speed and the kerf width required for efficient melt ejection from the cut kerf. Focal point positions located away from the workpiece top surface—either above the workpiece top surface or close to

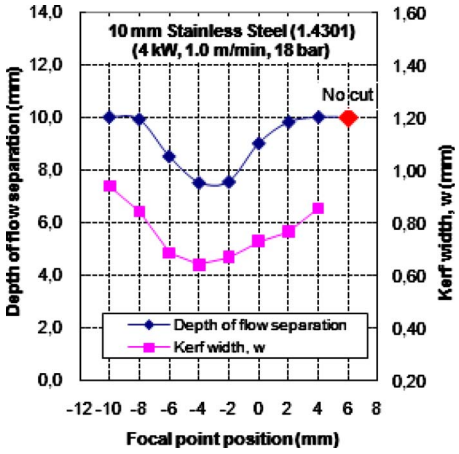

FIG. 8. Depth of flow separation and kerf width variation with focal point position.

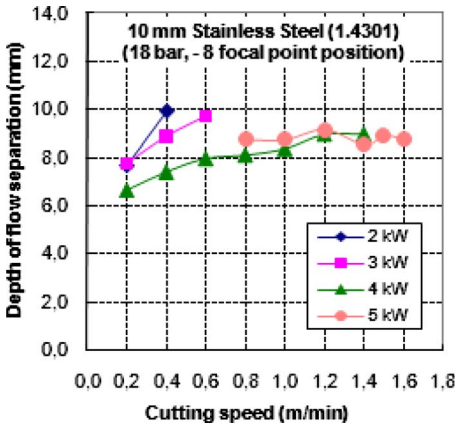

FIG. 9. Depth of flow separation with cutting speed.

the bottom surface of the workpiece—give a larger focused beam size on the workpiece and produce wider cut kerfs which enhance the melt flow velocity in the cut kerf so that the melt flow clears the bottom cut edge before flow separation occurs and with minimal dross attachment on the lower cut edge. However, the necessary condition for these focal point positions is that the power intensity on the workpiece should be sufficient to produce complete penetration of the workpiece.

F. Effect of cutting speed

The depth of flow separation moves closer to the bottom cut edge with increase in cutting speed (Fig. 9).

Higher dross attachment is obtained when lower cutting speeds are applied than during a faster cutting process (see Fig. 10). The high power loss from the cutting zone to the substrate material when cutting is performed with low cutting speeds results in lower melt temperature and high melt viscosity due to the temperature dependence of viscosity. This subsequently results in reduced melt removal rate at the lower cut section where there is melt buildup and high dross attachment on the lower cut edge [see Fig. 10(a)]. As the cutting speed is increased, the beam is more efficiently coupled to the workpiece and less power is lost from the cutting zone to the substrate material. Due to the reduced power losses during a fast laser cutting process, the melt temperature will be higher resulting in lower melt viscosity and better melt removal from the cut kerf with less dross attachment on the lower cut edge [see Fig. 10(b)].

V. CONCLUSIONS

The melt flow velocity and melt film thickness were formulated in this paper and correlated with the depth of flow separation on the cut edge in 10 mm stainless steel AISI 304 (EN 1.4301) workpiece. Good correlation was found between the calculated melt flow velocity and melt film thickness, with the depth of flow separation on the cut edge in the cutting experiments. A high cut edge quality is obtained when the assist gas pressure is sufficient to sustain a laminar boundary layer throughout the entire cut thickness so that the

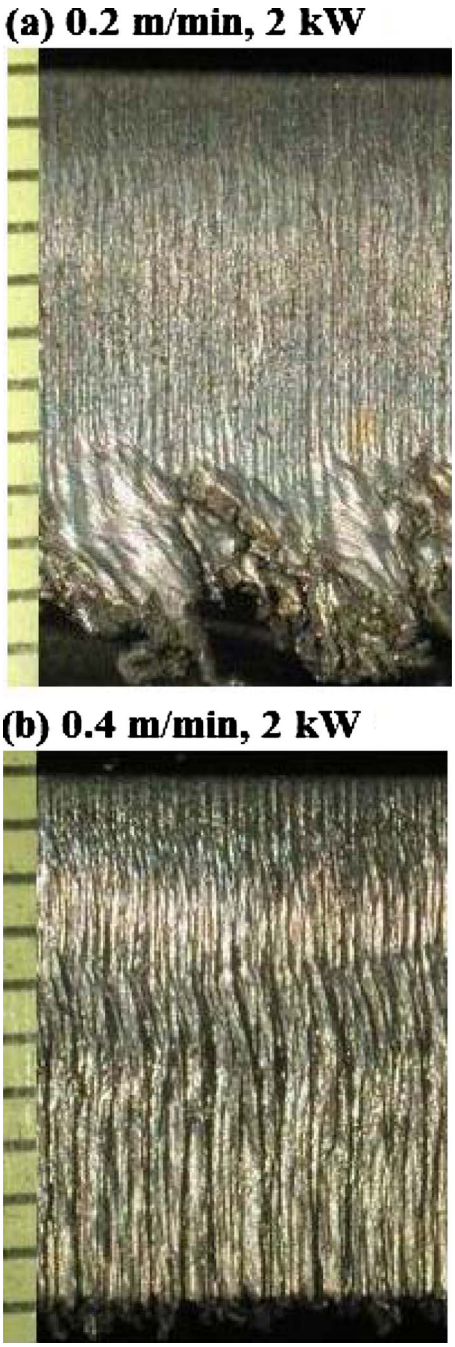

FIG. 10. Effect of cutting speed on dross attachment.

melt flow clears the cut edge without the occurrence of flow separation and with minimal dross attachment on the lower cut edge.

The cutting parameters that have a significant influence on the rate of melt removal from the cut kerf during thick-section stainless steel laser cutting using an inert assist gas include the assist gas pressure, nozzle diameter, focal point position, and cutting speed. A high rate of melt removal from the cut kerf and subsequently high cut edge quality can be achieved with the following cutting conditions:

High assist gas pressure (>16 bar in 10-mm-thick workpiece).
Large nozzle diameter (e.g., 2.5 mm nozzle).
Focal point position located close to the workpiece bottom surface so as to create a larger cut kerf width.
Optimum cutting speed to prevent dross attachment on the lower cut edge.

ACKNOWLEDGMENTS

The authors express their gratitude to the company HT LaserTekniikka Oy for funding this work. Pertti Kokko's effort in performing the cutting tests is highly appreciated.

[1]F. O. Olsen, "Fundamental mechanisms of cutting front formation in laser cutting," Proc. SPIE **2207**, 235–247 (1994).
[2]F. O. Olsen, "Cutting front formation in laser cutting," CIRP Ann. **38**, 215–218 (1989).
[3]B. T. Rao and A. K. Nath, "Melt flow characteristics in gas-assisted laser cutting," Sadhana: Proc., Indian Acad. Sci. **27**, 569–575 (2002).
[4]M. S. Gross, S. Celotto, and W. O'Neill, "Melt flow in narrow thick section kerfs," *ICALEO 2006 Congress Proceedings, Scottsdale, Arizona* (Laser Institute of America, Orlando, 2006), Paper 403, 206–210.
[5]M. Sparkes, M. Gross, S. Celotto, T. Zhang, and W. O'Neill, "Inert cutting of medium section stainless Steel using a 2.2 kW high brightness fiber laser," *ICALEO 2006 Congress Proceedings, Scottsdale, Arizona* (Laser Institute of America, Orlando, 2006), Paper 402, 197–205.
[6]M. Sparkes, M. Gross, S. Celotto, T. Zhang, and W. O'Neill, "Practical and theoretical investigations into inert gas cutting of 304 stainless steel using a high brightness fiber laser," J. Laser Appl. **20**, 59–67 (2008).
[7]J. Duan, H. C. Man, and T. M. Yue, "Simulation of high pressure gas flow field inside a laser cut kerf," *Proceedings of ICALEO 2000 Section B* (Laser Institute of America, Orlando, 2000), pp. 87–96.
[8]G. Tani, L. Tomesani, and G. Campana, "Prediction of melt geometry in laser cutting," Appl. Surf. Sci. **208–209**, 142–147 (2003).
[9]H. C. Man, J. Duan, and T. M. Yue, "Behavior of supersonic and subsonic gas jets inside laser cut kerfs," *Proceedings of ICALEO 1997 Section B* (Laser Institute of America, Orlando, 1997), pp. 27–36.
[10]H. C. Man, J. Duan, and T. M. Yue, "Design and characteristic analysis of supersonic nozzles for high gas pressure laser cutting," J. Mater. Process. Technol. **63**, 217–222 (1997).
[11]K. Chen, Y. L. Yao, and V. Modi, "Gas jet: Workpiece interactions in laser machining," ASME J. Manuf. Sci. Eng. **122**, 429–438 (2000).
[12]J. Fieret, M. J. Terry, and B. A. Ward, "Overview of flow dynamics in gas assisted laser cutting," *Paper presented at the Fourth International Symposium on Optical and Optoelectronic Applied science and Engineering, Topical Meeting on High Power Lasers: Sources, Laser-Material Interactions, High Excitations, and Fast Dynamics in Laser Processing and Industrial Applications, The Hague, The Netherlands* (SPIE, Bellingham, WA, 1987), pp. 243–250.
[13]H. Jun, S. Guo, L. Lei, and Z. Yao, "Characteristics analysis of supersonic impinging jet in laser machining," Int. J. Adv. Manuf. Technol. **39**, 716–724 (2008).
[14]D. Leidinger, A. Penz, and D. Schöcker, "Improved manufacturing processes with high power lasers," Infrared Phys. Technol. **36**, 251–266 (1995).
[15]H. C. Man, J. Duan, T. M. Yue, and P. Dong, "Design of supersonic nozzle for laser cutting with high pressure gas," *Proceedings of ICALEO 1997 Section B* (Laser Institute of America, Orlando, 1997), pp. 118–127.
[16]H. C. Man, J. Duan, and T. M. Yue, "Dynamic characteristics of gas jets from subsonic and supersonic nozzles for high pressure gas laser cutting," Opt. Laser Technol. **30**, 497–509 (1998).
[17]F. Quintero, J. Pou, J. L. Fernández, A. F. Doval, F. Lusquiños, M. Boutinguiza, R. Soto, and M. Perez-Amor, "Optimization of an off-axis nozzle for assist gas injection in laser fusion cutting," Opt. Lasers Eng. **44**, 1158–1171 (2006).
[18]A. Riveiro, J. Pou, F. Lusquiños, M. Boutinguiza, F. Quintero, R. Soto, R. Comesaña, and M. Perez-Amor, "Laser cutting of 2024-T3 aeronautic aluminium alloy," *ICALEO 2006 Congress Proceedings* (Laser Institute of America, Orlando, 2006), Paper 406, 225–232.
[19]J. Duan, H. C. Man, and T. M. Yue, "Modeling the laser fusion cutting process: III. Effects of various process parameters on cut kerf quality," J. Phys. D **34**, 2143–2150 (2001).
[20]Kai Chen, Y. Lawrence Yao, and Vijay Modi, "Gas dynamic effects on laser cut quality," J. Manuf. Process. **3**, 38–49 (2001).

[21]W. Schulz, V. Kostrykin, M. Nießen, J. Michel, D. Petring, E. W. Kreutz, and R. Poprawe, "Dynamics of ripple formation and melt flow in laser beam cutting," J. Phys. D **32**, 1219–1228 (1999).
[22]"Properties and concepts of single fluid flows," in *Encyclopedia of Fluid Mechanics Volume 1: Flow Phenomena and Measurement*, edited by N. P. Cheremisinoff (Gulf, Houston, 1986), ISBN: 0-87201-513-0, pp. 278–287.
[23]J. M. Kay and R. M. Nedderman, "Equations of motion for a viscous fluid," *An Introduction to Fluid Mechanics and Heat Transfer*, 3rd ed. (Cambridge University Press, Cambridge, 1974), pp. 150–157.
[24]M. Vicanek and G. Simon, "Momentum and heat transfer of an inert gas jet to the melt in laser cutting," J. Phys. D **20**, 1191–1196 (1987).
[25]T. Zacharia, S. A. David, J. M. Vitek, and H. G. Kraus, "Computational modeling of stationary gas-tungsten-arc weld pools and comparison to stainless steel 304 experimental results," Metall. Trans. B **22**, 243–257 (1991).
[26]Anon., http://encyclopedia.airliquide.com, Accessed March 22, 2010.